Task 3.2

Title

Computational energy innovation

Projects (presented on the following pages)

GPU-accelerated Finite Volume Particle simulation of multi-jet Pelton Turbine Flow
S. Alimirzazadeh, S. Leguizamón, T. Kumashiro, K. Tani, F. Avellan

Turbulence modeling for extendedoperating-range of hydraulic machines
A. Del Rio, E. Casartelli, L. Mangani, D. Roos Launchbury

Multiscale Simulation of Prototype-Scale Pelton Turbine Erosion
Sebastián Leguizamón, Siamak Alimirzazadeh, François Avellan

Simulations of transport phenomena in porous media on non-conforming meshes
Maria Giuseppina Chiara Nestola, Marco Favino, Patrick Zulian, Klaus Holliger, Rolf Krause

Fictitious domain methods for HMprocesses in fractures
Cyrill von Planta, Daniel Vogler, Xiaqing Chen, Maria Nestola, Martin O. Saar, Rolf Krause

Non-conforming mesh models for flow in fractured porous media using the method of Lagrange multipliers
Patrick Zulian, Philipp Shäddle, Daniel Vogler, Maria Nestola, Liudmila Karagyaur, Sthavishtha Bhopalam, Anozie Ebigbo, Martin Saar, Rolf Krause

SCCER SoE
SWISS COMPETENCE CENTER for ENERGY RESEARCH
SUPPLY of ELECTRICITY

SCCER-SoE Annual Conference 2019

LMH Laboratory for Hydraulic Machines
EPFL

In cooperation with the CTI
Energy
Swiss Competence Centers for Energy Research
Schweizerische Eidgenossenschaft
Confédération suisse
Confederazione Svizzera
Confederaziun svizra
Swiss Confederation
Commission for Technology and Innovation CTI

GPU-accelerated Finite Volume Particle simulation of multi-jet Pelton Turbine Flow

S Alimirzazadeh, S Leguizamón, T Kumashiro, K Tani, F Avellan

GPU-SPHEROS

GPU-SPHEROS is a GPU-accelerated particle-based versatile solver based on Arbitrary Lagrangian Eulerian (ALE) Finite Volume Particle Method (FVPM) which inherits desirable features of both Smoothed Particle Hydrodynamics (SPH) and mesh-based Finite Volume Method (FVM) and is able to simulate the interaction between fluid, solid and silt [1]. With GPU-SPHEROS, the goal is to perform industrial size setup simulations of hydraulic machines.

Multi-jet Pelton Simulation

Multi-jet Pelton turbines are popular for their flexibility in covering a wide operating range including high specific speeds. However, with by increasing the number nuzzles, there is a higher risk of jet interference which can cause a sudden efficiency drop. GPU-SPHEROS, as particle-based solver is used to simulating a six-jet Pelton turbine flow in a wide operating range including the Best Efficiency Point (BEP) and off-design conditions. The jet interference inception range is then predicted and validated by the experiments performed by Hitach-Mitsubishi Hydropower systems.

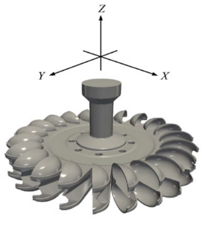

Geometry

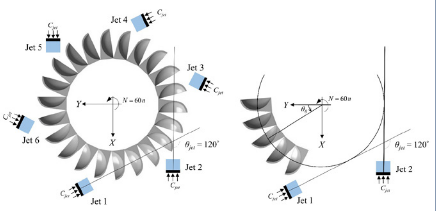

Six-jet simulation setup

Validation for Turbulent Impinging Jet on a Flat Plate

- A turbulent fluid jet impinging on a flat plate has been validated for pressure and free surface elevation against available experimental data for non-uniform jet velocity profile. As a case study with close hydrodynamics to Pelton turbine.
- The validated solver has been then used for multi-jet Pelton flow simulation.

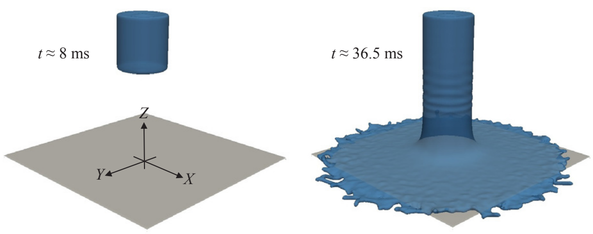

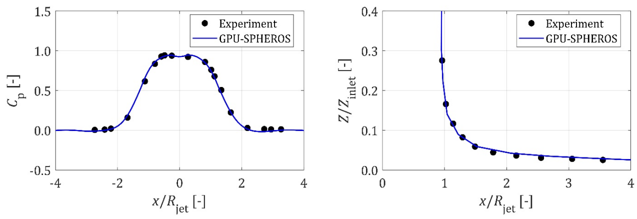

Dual-jet Simulation Setup

- A dual-jet simplified simulation setup is used to investigate the interaction between the adjacent jets at eight different operating points N/N_{BEP} = $\{0.89, 0.94, 1.0, 1.05, 1.11, 1.16, 1.22, 1.31\}$ where N is the runner rotational speed in min $^{-1}$ and BEP is the Best Efficiency Point.
- The free surface has been reconstructed and visualized in Paraview open source data analysis software.
- Even though the torque is underestimated, the trend is in a very good agreement with the experiment.

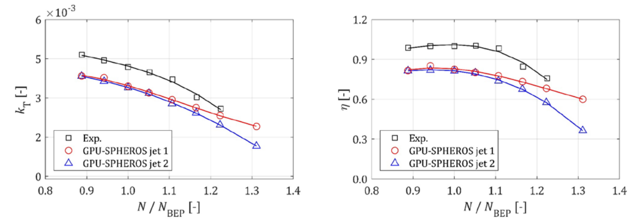

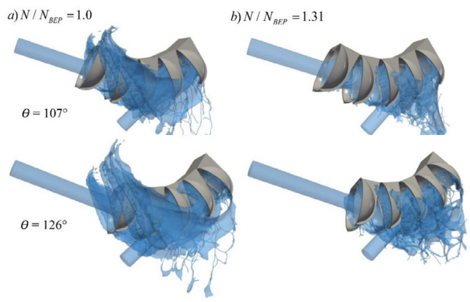

Six-Jet Full Pelton Flow Simulation

- A six-jet full Pelton flow has been simulated with GPU-SPHEROS on 12 GPUs to investigate and track the free surface and jet interactions.
- The solver is able to robustly handle industrial size problems with a violent free surface.

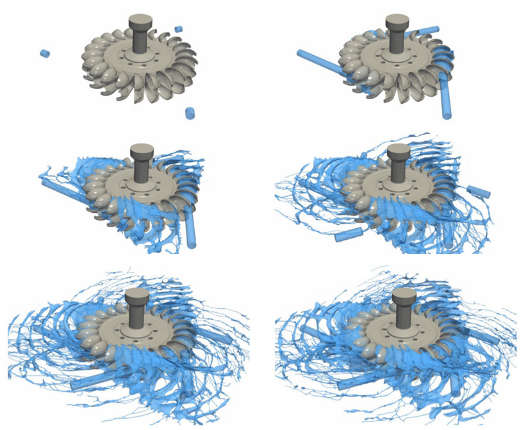

References

S Alimirzazadeh, E Jahanbakhsh, A Maertens, S Leguizamon, F Avellan, GPU-Accelerated 3-D finite volume particle method, *Computers & Fluids*. 171 (2018) 79–93

Experimental data is provided by “Kvicinsky S. Kvicinsky, Methode d'analyse des Ecoulements 3D a Surface Libre: Application aux Turbines Pelton, École Polytechnique Fédérale de Lausanne, doctoral Thesis N° 2526 2002»

SCCER-SoE Annual Conference 2019

SCCER SoE
SWISS COMPETENCE CENTER for ENERGY RESEARCH
SUPPLY of ELECTRICITY

Supported by:
Schweizerische Eidgenossenschaft
Confédération suisse
Confederazione Svizzera
Confederaziun svizra
Swiss Confederation
Innosuisse – Swiss Innovation Agency

Lucerne University of Applied Sciences and Arts
HOCHSCHULE LUZERN
Technik & Architektur

Turbulence modeling for extended operating-range of hydraulic machines

A. Del Rio, E. Casartelli, L. Mangani, D. Roos Launchbury

Introduction

Hydropower plants are very well suited for the modern electricity market which depends on high flexibility and storage capabilities. In order for pump turbines to fulfill todays requirements, favorable stable behavior over a large range of guide vane openings (GVO's) is necessary. This includes operation points (OP's) from turbine start (GVO3°) and synchronization (GVO6°) all the way to regular operation and part/over-load (GVO ~ 20°).

Simulations of unstable off-design conditions are difficult to perform, because the conditions are dominated by turbulent vortex structures in the vaneless space, which often cannot be accurately predicted using conventional turbulence models. This is due to the fact that the most commonly used models, such as k-epsilon and the Shear Stress Transport (SST) model assume *isotropic turbulence*. This assumption is not valid for many flow problems but seems to have an especially large influence in pump turbine instability simulations.

The goal of the current efforts is to investigate and compare the performance of various turbulence models at off-design conditions over a broad range of GVO's. The standard eddy viscosity models SST k-omega and k-epsilon are thereby compared with more advanced turbulence models.

CFD Setup

- Full-size pump-turbine prototype
- Computational domain includes Volute & Stay Vanes (A), Guide Vanes (GV, B), Runner (C) and Draft Tube (D) shown in Fig. 1
- In-house, coupled, unsteady solver with efficient moving-mesh Capabilities
- Investigated Turbulence models: k-epsilon, SST k-omega, Explicit Algebraic Reynolds Stress Model (EARSM)

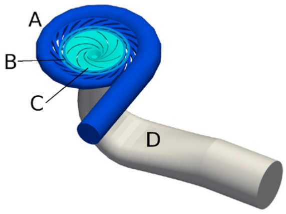

Figure 1: Computational domain

EARS models do not solve for additional transport equations but try to reconstruct the unknown stress tensor through an algebraic equation based on the strain rate, vorticity and the turbulent time-scale [1]. The implemented model is based on [2][3] and uses the baseline (BSL) k-omega model to calculate the turbulent time-scale.

Results

Fig. 2 shows the four quadrant characteristic for load rejection, a sort of emergency shutdown of the pump-turbine. The GVO are thereby decreased from 24° to 6°, which leads to oscillations in the operation mode between turbine-brake and reverse-pump.
As can be seen from Fig. 2 all three turbulence models are in good agreement with the reference curve for large GVO's (~20°). For GVO6° only k-epsilon and BSL EARSM are capable of capturing the positive slope in the S-shape according to the reference curve.

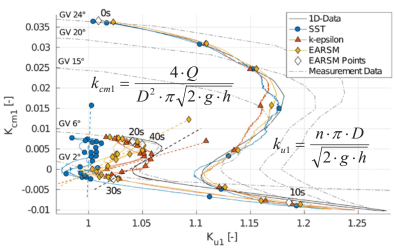

Figure 2: Influence of the turbulence model on the simulated stability characteristic for large GVO angles (~20°) and for the synchronisation angle of 6°

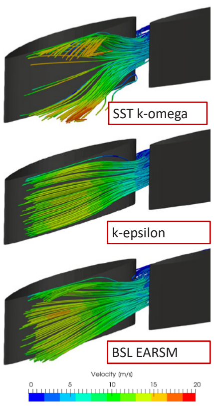

Figure 3: 3D Velocity-streamlines for GVO6°

SST k-omega produces almost a stable characteristic. Fig. 3 shows the flow behavior in the GV channel and vaneless space for all three turbulence models. The SST k-omega model overestimates the separation behavior on the GV blades, which leads to horseshoe type vortices. These structures seem to have a stabilizing effect on the simulation. BSL EARSM and k-epsilon on the other hand produce less separation.

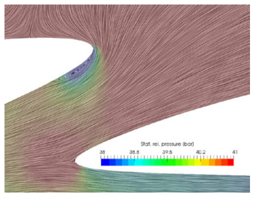

Figure 4: LIC velocity plot through the GV channel for GVO6°

During the process of turbine-start (Fig. 5) the GVO is increased from 1° to a final value of 3°. For these small openings operates the pump-turbine in a stable way, which can be reproduced with SST k-omega and BSL EARSM. The k-epsilon model on the other hand produces still and instability as can be seen from Fig. 5. The smaller GVO leads to more incidence at the GV LE (Fig. 4), which produces strong horseshoe type vortices for the SST k-omega and BSL EARSM simulations (Fig. 6). These vortices seem again to have a stabilizing effect on the simulation.

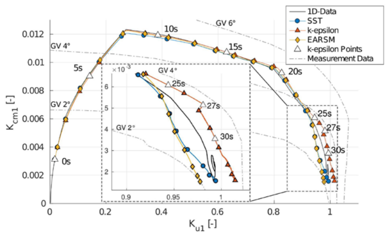

Figure 5: Influence of the turbulence model on the simulated stability characteristic for a small GVO angle of 3°

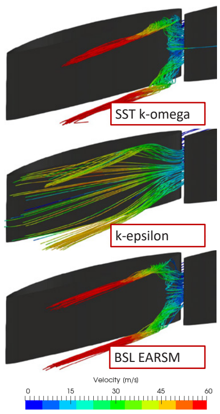

Figure 6: 3D Velocity-streamlines for GVO3°

Discussion

The benefits of the anisotropic BSL EARSM turbulence model have been presented for pump-turbine simulations under unstable off-design conditions. Although for certain GVO's it is possible to produce good results with k-epsilon and/or SST k-omega, only BSL EARSM guarantees consistently good results for all investigated GVO's. In addition, the better numerical performance can be partly explained physically. The higher complexity of BSL EARSM allows for example the capturing of turbulence driven secondary flow, which provides the low-energy boundary layer flow with momentum and prevents the flow from separation. This effect is one of the main causes, why BSL EARSM produces better results for the load rejection case (Fig. 2) compared to SST k-omega. K-epsilon on the other hand provides no physical explanation for its superiority compared to SST k-omega in this case.

In the upcoming research additional operating cases will be considered and further turbulence models will be investigated. Of special interest are the full Reynolds-Stress model (RSM) and 4-equation models with focus on elliptic blending. The available RS-model is implemented in coupled form in the in-house code of the CC FMHM. The coupling improves the stability behavior drastically, which makes the model suitable for the challenging pump-turbine simulations.

References

[1] Wallin, S., and Johansson, A., "An explicit algebraic Reynolds stress model for incompressible and compressible turbulent flows." Journal of Fluid Mechanics 403 (2000): 89-132.
[2] Hellsten, A., "New Advanced k-omega Turbulence Model for High-Lift Aerodynamics", AIAA Journal, Vol. 43, No. 9, 2005, pp. 1857-1869.
[3] Menter, F. R., Garbaruk, A.V., and Egorov, Y., "Explicit Algebraic Reynolds Stress Models for Anisotropic Wall-Bounded Flows", Progress in Flight Physics, Vol. 3, 2012, pp. 89-104

SCCER SoE
SWISS COMPETENCE CENTER for ENERGY RESEARCH
SUPPLY of ELECTRICITY

SCCER-SoE Annual Conference 2019

LMH Laboratory for Hydraulic Machines

EPFL

Supported by:
Schweizerische Eidgenossenschaft
Confédération suisse
Confederazione Svizzera
Confederaziun svizra

Swiss Confederation

Innosuisse – Swiss Innovation Agency

Multiscale Simulation of Prototype-Scale Pelton Turbine Erosion

Sebastián Leguizamón, Siamak Alimirzazadeh, François Avellan

Motivation and Problem Description

The hydro-abrasive erosion of turbomachines is a **significant problem** worldwide. In the context of the Energy Strategy 2050, it is a problem that will become **more severe in the future** due to the retreat of glaciers and permafrost caused by **climate change**.

The project objective is to deliver a numerical **simulation tool** with predictive power that may become **advantageous** for the **design** and the **operation** of the machines.

The erosion of hydraulic turbomachines is an **inherently multiscale process**; its simulation is therefore very complicated. It requires a multiscale modeling approach.

Multiscale Erosion Model

A multiscale model has been recently formulated by the authors [1]. It encompasses two submodels to tackle the multiscale character of the problem.

Microscale output
- Erosion ratio $f(\alpha_i, C_j)$
- Restitution coefficients $f(\alpha_i, C_j)$

Sequential coupling

Macroscale output
- Impact condition distributions
- Sediment flux against the surface
- Erosion distribution
- Global erosion rate

In the **Microscale Model**, detailed impact simulations are performed taking into consideration all the important physical effects. These simulations result in the **erosion ratio** for each impact condition studied.

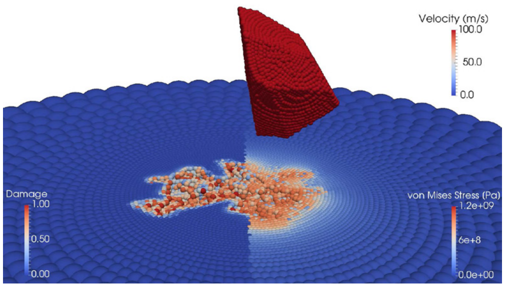

Microscale simulation: Sediment impacting a solid specimen.

In the **Macroscale Model**, the turbulent sediment transport is computed; each time a sediment impact is detected, the results of the microscale simulations are interpolated, resulting in the macroscopic **erosion accumulation**.

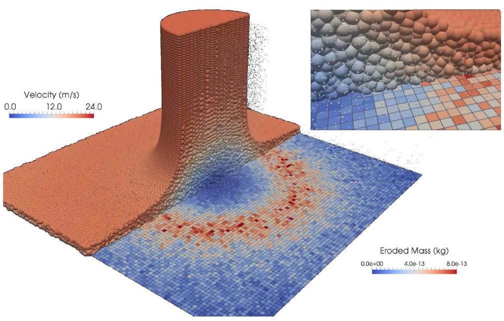

Macroscale simulation: Slurry jet eroding a flat plate.

Case Study Description

The model has been previously validated on a laboratory-scale case [1] and on a fixed Pelton bucket [2]. Now, a **prototype-scale Pelton turbine** case study is used for further **validation**.

The 84 MW turbine has a pitch diameter D_1 = 2.87 m, and features 21 buckets and 6 jets.

The study period lasts 21 months during which characterizations of the sediments and the turbine erosion have been performed.

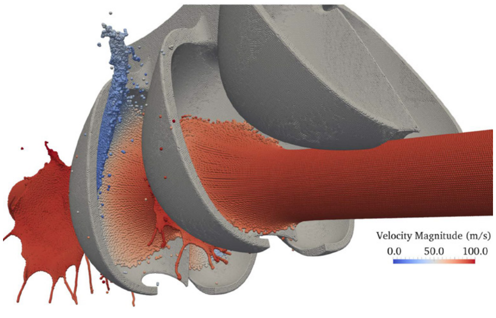

Discretization of the jet impinging on the Pelton turbine.

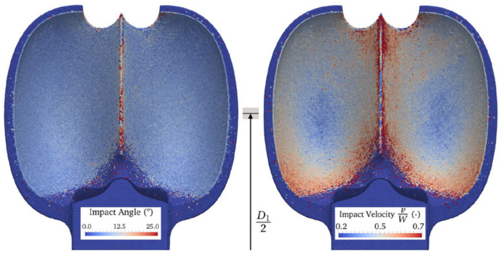

Average impact angle and velocity distributions.

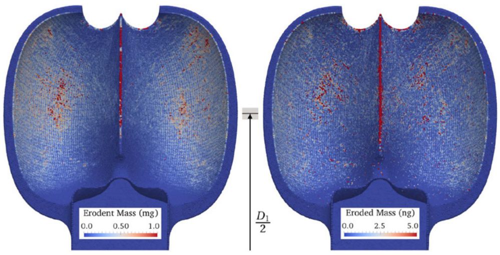

Impacted sediment mass and eroded mass distributions.

Simulation Results

The macroscale simulation yields important information that may be used to understand the erosion process.

For instance, the average **impact conditions** shown on the left, namely the sediment impact **angle** and **velocity**, are directly related to the material-dependent erosion magnitude.

Similarly, the **sediment flux** against the bucket wall, shown on the left, is determined by the sediment characteristics such as its size distribution, and by the local bucket curvature.

These three distributions are the culprit of the **eroded mass** distribution, also presented on the left, and may therefore shed some light on the erosion phenomenon.

Validation of the Erosion Predictions

The simulation results were validated with the experimental **erosion depth** available for each bucket, at the points D_i, O_i and sections S_i shown on the right, and with the experimental **total eroded mass**.

As shown below, the **average relative error** is 35% for the pointwise comparisons, 14% for the sectional comparisons, and only 4% for the total eroded mass.

The **modeling error** has been estimated at **26%±24%** based on these results and the experimental uncertainty.

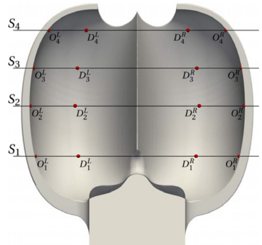

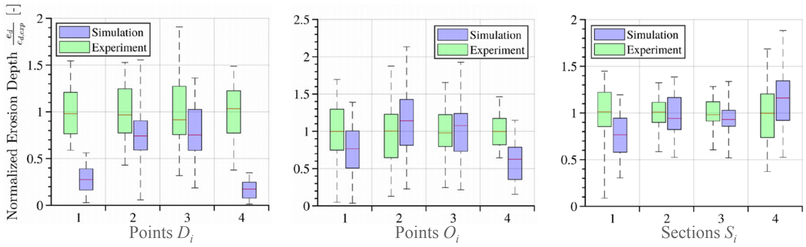

Comparison of simulated and measured erosion depth at eight points and across four sections.

References

[1] S. Leguizamón, E. Jahanbakhsh, A. Maertens, S. Alimirzazadeh, F. Avellan, A multiscale model for sediment impact erosion simulation using the finite volume particle method, *Wear* 392-393 (2017).

[2] S. Leguizamón, E. Jahanbakhsh, S. Alimirzazadeh, A. Maertens, F. Avellan, Multiscale simulation of the hydroabrasive erosion of a Pelton bucket: Bridging scales to improve the accuracy, *International Journal of Turbomachinery, Propulsion and Power* 4 (2019) 9.

SCCER SoE
SWISS COMPETENCE CENTER for ENERGY RESEARCH
SUPPLY of ELECTRICITY

SCCER-SoE Annual Conference 2019

Supported by:
Schweizerische Eidgenossenschaft
Confédération suisse
Confederazione Svizzera
Confederaziun svizra
Swiss Confederation
Innosuisse – Swiss Innovation Agency

Simulations of transport phenomena in porous media on non-conforming meshes

Maria Giuseppina Chiara Nestola, Marco Favino, Patrick Zulian, Klaus Holliger, Rolf Krause

Introduction

Numerical simulations of fluid flow and transport **in fractured porous media** is a challenging problem due to the different scales involved. In fact, the fracture width tends to be **orders-of-magnitude** smaller than the characteristic size of the embedding matrix. Due to this difference, the creation of computational meshes that explicitly resolve fractures remains an immensely complicated and tedious task, which, so far, is possible only for small numbers of fractures.

In order to allow for the numerical simulation of complicated fracture networks, **hybrid-dimensional approaches** have been developed [1]. In contrast to **equi-dimensional** ones, where fractures are **three-dimensional objects**, fractures, due to their aspect ratio, are described as **lower-dimensional objects**, whose width is modeled as a coefficient in the equations and suitable coupling conditions between the fractures and the embedding matrix are imposed.

Although, **hybrid-dimensional approaches** have been widely employed for the simulation of rather complicated media, a comparison with **equi-dimensional approaches** has never been performed for **transport problems** in fractured media. In this work, we consider the case of a regular fracture network, whose computational mesh for the hybrid model can be generated employing an adaptive mesh refinement technique [2]. For both approaches, we compare the results of the simulations of fluid flow and transport.

Methods

Equi-dimensional model

The matrix and the fractures have the same spatial dimension, thus allowing for a full characterization of the geometrical features.

Fluid flow

$$\begin{aligned} -\nabla\cdot\mathcal{K}\nabla P &= 0 \ \text{ in } \Omega \\ P &= \bar{p} \text{ on } \Gamma^D \\ -\mathcal{K}\nabla P\cdot n &= \bar{J} \text{ on } \Gamma^N \end{aligned}$$

Transport

$$\begin{aligned} \phi\frac{\partial c}{\partial t} + \nabla(c\tilde{u}) &= 0 \ \text{ in } \Omega \\ c &= \bar{c} \ \text{ on } \Gamma^c \end{aligned}$$

$$\tilde{u} = -\mathcal{K}\nabla P$$

$$\int_\Omega \mathcal{K}\nabla P^h\cdot\nabla v^h\, dV - \int_{\Gamma^N} \bar{J} v^h\, dS = 0 \qquad \int_\Omega \phi\frac{\partial c^h}{\partial t} w^h\, dV + \int_\Omega \tilde{u}\cdot\nabla c^h w^h\, dV = 0$$

The embedded fractures are defined as subsets of the domain, for which different values of the permeability and porosity are assigned.

Hybrid-dimensional model

The fractures have a lower spatial dimension than the matrix. The equations for the fractures are obtained by averaging across the fractures.

Fluid flow

$$\begin{aligned} -\nabla\cdot K_i\nabla P_i &= 0 \ \text{ in } \Omega_i \\ P_i &= \bar{p}_i \text{ on } \Gamma_i^D \\ -K_i\nabla P_i\cdot n_i &= \bar{J}_i \text{ on } \Gamma_i^N \end{aligned}$$

Transport

$$\begin{aligned} \phi_i\frac{\partial c_i}{\partial t} + \nabla(c_i\tilde{u}_i) &= 0 \ \text{ in } \Omega_i \\ c_i &= \bar{c}_i \ \text{ on } \Gamma_i^c \end{aligned}$$

i={m,f}, with m referring to the matrix and f to the fractures

$$\begin{aligned} \int_\Omega K_m\nabla P_m^h\cdot\nabla v_m^h\, dV - \int_{\Gamma^N}\bar{J}_m v_m^h\, dS - \int_\gamma \lambda^h v_m^h\, dS &= 0 \\ \int_\omega K_f\nabla P_f^h\cdot\nabla v_f^h\, dV - \int_{\gamma^N}\bar{J}_f v_f^h\, dS + \int_\gamma \lambda^h v_f^h\, dS &= 0 \\ \int_\gamma (\mathbf{P}_f^h - \mathbf{P}_m^h)\,\mu^h\, d\mathbf{S} &= \mathbf{0} \end{aligned}$$

$$\begin{aligned} \int_\Omega \phi_m\frac{\partial c_m^h}{\partial t} w_m^h\, dV + \int_\Omega \tilde{u}_m^h\cdot\nabla c_m^h w_m^h\, dV - \int_\gamma \lambda^h w_m^h\, dS &= 0 \\ \int_\omega \phi_f\,\epsilon\frac{\partial c_f^h}{\partial t} w_f^h\, dV + \int_\omega \tilde{u}_f^h\cdot\nabla c_f^h w_f^h\, dV + \int_\gamma \lambda^h w_f^h\, dS &= 0 \\ \int_\gamma (\mathbf{c}_f^h - \mathbf{c}_m^h)\,\mu^h\, d\mathbf{S} &= \mathbf{0} \end{aligned}$$

Lagrange multipliers are used to apply **coupling conditions** at the interfaces between the matrix and the fractures [3]. These additional equations are denoted in red.

Discretization and stabilization Technique

For both approaches, we employed first-order finite element methods. To ensure the stability of the discretization and the positivity of the solution, we employed a Flux Correction Transport technique [4].

Results

For both approaches, we compare
- pressure distribution for the flow problem,
- concentration for the transport problem.

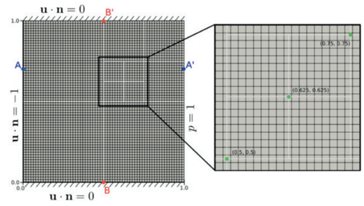

The considered domain is a unitary square with 6 fractures [1], whose width is four orders-of magnitude smaller of the domain size. For the hybrid-dimensional model, we employ a fine mesh with 0.6 millions of elements, while for the equi-dimensional approach, we consider four different mesh resolutions.

Fluid flow | **Transport**

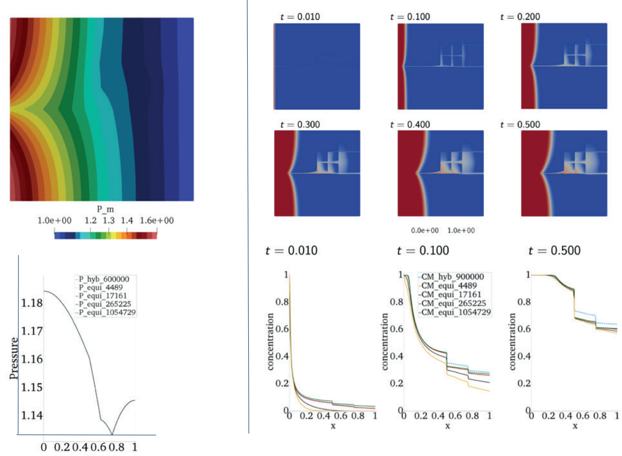

Top row: **pressure distribution** of the flow problem (left) and **concentration** at six different time-steps for the transport problem (right). Both solutions have been computed using the equi-dimensional model. Bottom row: comparison of **pressure distribution** (left) and **concentration** at three different time steps (right) between hybrid- and equi-dimensional approaches along the line y=0.5.

Discussion

Flow problem: No relevant differences between **hybrid-** and **equi-dimensional** approaches. Both are able to reproduce the reference solution [1].

Transport problem: Hybrid-dimensional approach reproduces the reference solution. In particular, the vertical drop in the concentration at x=0.5 is bounded. On the other hand, in the **equi-dimensional** approach the vertical drop increases over time. At the final simulation time, we observe that the two approaches have converged to different solutions. This may be due to lower cross-fracture transport for the **hybrid-dimensional** model, which, in turn, would suggest that the **equi-dimensional** approach **allows to describe features,** which a **hybrid-dimensional one doesn't account for.**

References

[1] Odsæter, Lars H., Trond Kvamsdal, and Mats G. Larson. *A simple embedded discrete fracture matrix model for a coupled flow and transport problem in porous media*. Computer Methods in Applied Mechanics and Engineering 343 (2019): 572-601.
[2] Hunziker, Jürg, et al. *Seismic attenuation and stiffness modulus dispersion in porous rocks containing stochastic fracture networks.* Journal of Geophysical Research: Solid Earth 123.1 (2018): 125-143.
[3] Schädle, Philipp, et al. *3D non-conforming mesh model for flow in fractured porous media using Lagrange multipliers.* arXiv preprint arXiv:1901.01901 (2019)
[4] Kuzmin, Dmitri. *Algebraic Flux Correction I. Scalar conservation laws.* Flux-corrected transport. Springer, Berlin, Heidelberg, 2005. 155-206. APA

SCCER-SoE Annual Conference 2019

SCCER SoE
SWISS COMPETENCE CENTER for ENERGY RESEARCH
SUPPLY of ELECTRICITY

Supported by:
Schweizerische Eidgenossenschaft
Confédération suisse
Confederazione Svizzera
Confederaziun svizra
Swiss Confederation
Innosuisse – Swiss Innovation Agency

Fictitious domain methods for HM-processes in fractures

Cyrill von Planta[1], Daniel Vogler[2], Xiaqing Chen[2], Maria Nestola[1], Martin O. Saar[2], Rolf Krause[1]
[1]Institute of Computational Science, Università della Svizzera Italiana
[2]Institute of Geophysics, ETH Zurich

Introduction

Fluid flow in rough fractures and the coupling with the mechanical behaviour of the fractures pose great difficulties for numerical modelling approaches, due to complex fracture surface topographies, the nonlinearity of hydromechanical processes and their tightly coupled nature.

Fictitious Domain Method

We have adapted a fictitious domain method to simulate hydromechanical processes in fracture-intersections. The solid is immersed in the fluid. The solid and fluid are simulated on separately and coupled with L^2-projections which can transfer information between non-conforming meshes. We use finite elements, linear elasticity, and the incompressible Navier-Stokes equations.

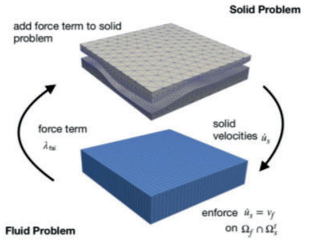

Figure: Schematic FD method. The full problem is solved in a fixed point iteration.

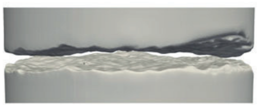

Figure: Contact surfaces within the fracture. Simulating contact is highly complex because nonmatching surfaces meshes must be properly related to each other.

Dual Mortar Method for Contact

Within the solid problem we simulate a two-body contact problem. We developed a dual mortar method to resolve the non-matching surfaces at the contact boundaries.

2D Intersection

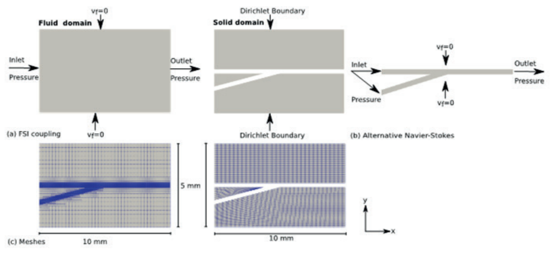

Figure: Setup of the benchmark meshes.

With the 2D intersection benchmark we validated our FD approach against a fluid simulation using only the Navier Stokes equations but with the same fluid-solid boundary.

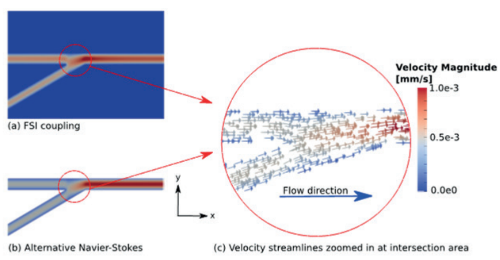

Figure: Left: Fluid velocity of FD approach is the same as in the alternative setup. Right: Acceleration of fluid velocities at channel intersection.

Governing equations

Solid: $\rho_s \ddot{u}_s - \mathrm{div}\sigma(u_s) = f_s \quad \text{on } \Omega^t_{s,1} \cup \Omega^t_{s,2},$

$$u_s = 0 \quad \text{on } (\Gamma^t_s)^D,$$

$$\sigma(u_s) \cdot n_s = h_s \quad \text{on } (\Gamma^t_s)^N,$$

Contact conditions: $\sigma_n \leq 0 \quad \text{on} \quad (\Gamma^t_{s,2})^C,$

$$\sigma_n(u_{s,1} \circ \Phi) = \sigma_n(u_{s,2}) \quad \text{on} \quad (\Gamma^t_{s,2})^C,$$

$$[u] \leq g \quad \text{on} \quad (\Gamma^t_{s,2})^C,$$

$$([u] - g)\sigma_n(u_{s,2}) = 0 \quad \text{on} \quad (\Gamma^t_{s,2})^C,$$

$$\sigma_T = 0 \quad \text{on} \quad (\Gamma^t_{s,2})^C.$$

Fluid: $\rho_f \dot{v}_f + \rho_f (v_f \cdot \nabla) v_f - \mu_f \nabla \cdot \sigma_f(p_f, v_f) = f_{\mathrm{fsi}} \text{ on } \Omega_f$

$$\nabla \cdot v_f = 0 \quad \text{on } \Omega_f$$

Coupling: $\dot{u}_s = v_f$

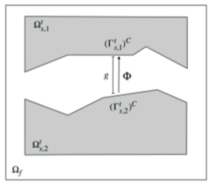

Fluid Flow in intersecting fracture

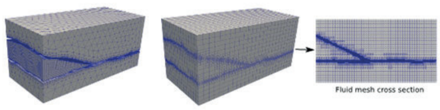

Figure: Setup of the meshes. In the fluid mesh, the area within the fracture has been refined.

We created a realistic intersecting fracture using SynFrac and used the FD approach to simulate fluid flow under increasing normal load. The simulations results show, that increasing closure of the fracture planes coincides with increasing fluid flow channeling.

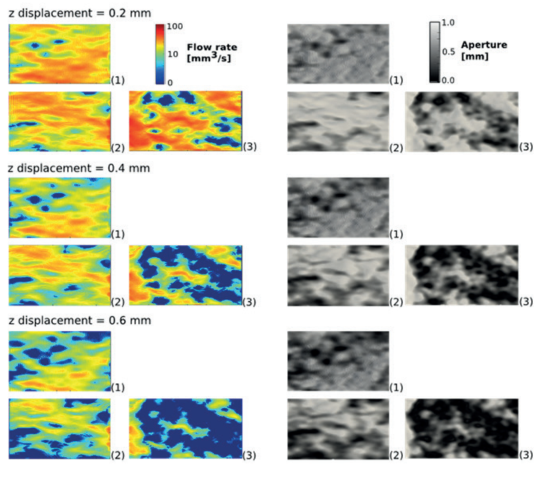

Figure: Left: flow rate under increasing load, measured in displacement of the top side of the fracture. Right: Aperture fields within the fracture.

Outlook

Fictitious domain methods combined with L^2 –projections are a highly promising tool to simulate geophysical processes. Next steps include the extension of the approach to nonlinear materials, thermal and other physical processes.

References

[1] Planta et. al. Simulation of hydro-mechanically coupled processes in rough rock fractures using an immersed boundary method and variational transfer operators. 2019. Comp. Geosciences.
[2] Planta et. al. Fluid-Structure Interaction with a parallel transfer operators to model hydro-mechanical processes in heterogeneous fractures. 2019. Special Issue Comp. Geosciences, submitted.
[3] Nestola et. al. An immersed boundary method for fluid-structure interaction based on variational transfer. J. of Comp. Phys. 2019

SCCER SoE

SWISS COMPETENCE CENTER for ENERGY RESEARCH
SUPPLY of ELECTRICITY

SCCER-SoE Annual Conference 2019

Supported by:

Schweizerische Eidgenossenschaft
Confédération suisse
Confederazione Svizzera
Confederaziun svizra

Swiss Confederation

Innosuisse – Swiss Innovation Agency

Non-conforming mesh models for flow in fractured porous media using the method of Lagrange multipliers

Patrick Zulian, Philipp Shäddle, Daniel Vogler, Maria Nestola, Liudmila Karagyaur, Sthavishtha Bhopalam, Anozie Ebigbo, Martin Saar, Rolf Krause

Motivation

- Flow through fracture networks is governed by **3D effects**
- **Mesh generation** of 3D fracture **networks** with conforming matrix **mesh** is very **challenging**

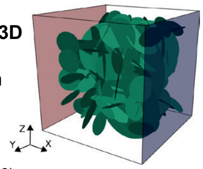

Our embedded non-conforming mesh approach

- Method of Lagrange multipliers (Köppel M. et al. 2018)
- **Variational transfer** operator (Krause R. & Zulian P. 2016)

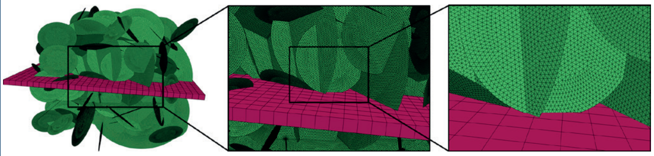

Article: Schädle P., Zulian P., Vogler D., Bhopalam S., Nestola M., Ebigbo A., Krause R., Saar M.
3D non-conforming mesh model for flow in fractured porous media using Lagrange multipliers,
Computers & Geosciences, 2019.

Method

Lagrange multiplier formulation

Flow in the porous-medium matrix, Ω

$$\nabla \cdot (-\mathbf{K}\nabla p) - \lambda = f \quad \text{in} \quad \Omega\,, \qquad p = 0 \quad \text{on} \quad \Gamma = \partial\Omega$$

Flow in the fracture, γ

$$\nabla_\gamma \cdot (-\mathbf{K}_\gamma \nabla_\gamma p_\gamma) + \lambda = f_\gamma \quad \text{in} \quad \gamma\,, \qquad p_\gamma = 0 \quad \text{on} \quad \Gamma = \partial\gamma$$

Find $(p, p_\gamma) \in \mathbf{V}$ and $\lambda \in \Lambda$, such that

$$\int_\Omega \mathbf{K}\nabla p \cdot \nabla q + \int_\gamma \mathbf{K}_\gamma \nabla_\gamma p_\gamma \cdot \nabla_\gamma q_\gamma - \int_\gamma \lambda(q - q_\gamma) = \int_\Omega fq + \int_\gamma f_\gamma q_\gamma\,, \qquad \forall (q, q_\gamma) \in \mathbf{V}$$

and

$$\int_\gamma (p - p_\gamma)\mu = 0\,, \qquad \forall \mu \in \Lambda$$

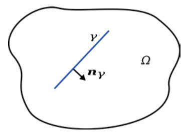

Matrix domain Ω with an embedded fracture domain γ and normal vector $\mathbf{n}$ on γ

The Lagrange multiplier represents the fluid pressure gradient $\lambda = \mathbf{K}\nabla p \cdot \mathbf{n}_\gamma$

Köppel, M. et al. (2018). *Computational Geosciences*, 1–15

Results: 2D validation

2D benchmarks from

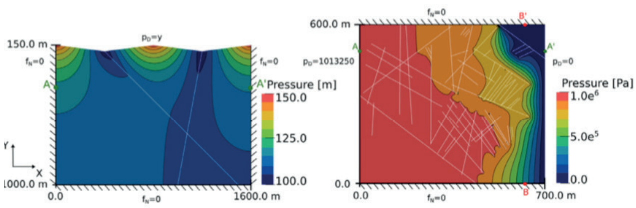

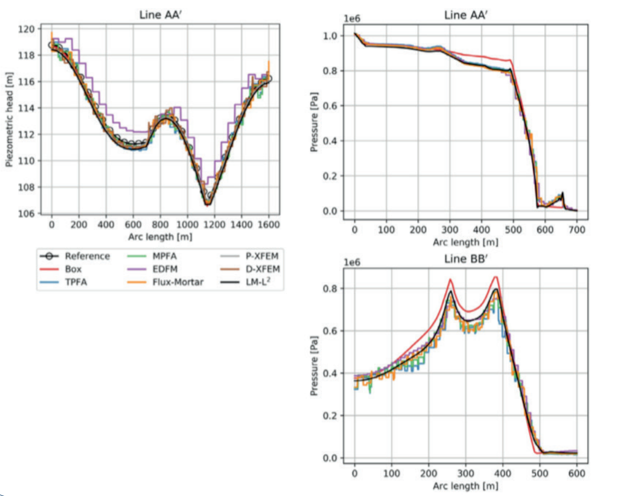

Results: 3D experiments

- Heterogeneous fracture network, error of embedded discretization

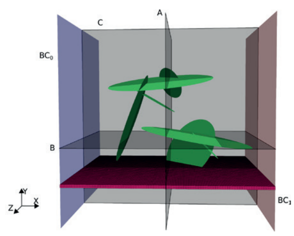

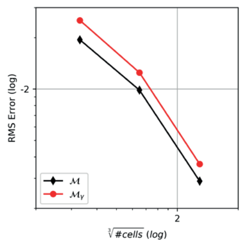

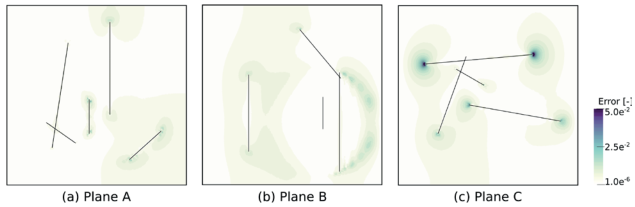

- Example with 150 randomly oriented fractures

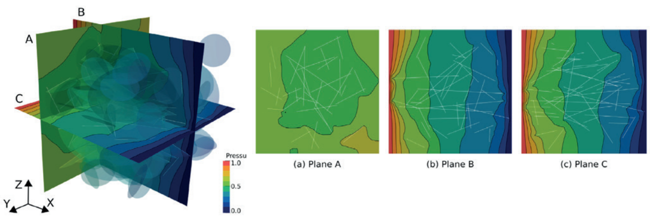

General information

- Simulation of fracture network for geothermal energy extraction
- Tool for automated generation of flow and transport in fracture networks
- Current status: equi- and hybrid-dimensional discretization for flow in 3D using the finite element method
- Simplification of the study of stochastic discrete fracture networks (DFN).
- DFNs necessary whenever the actual fracture network is not known

Conclusion

- Robust method with expected behaviour of the L^2—error
- Results in agreement with benchmarks present in the literature
- Suitable for **large-scale, realistic fracture network realizations in 3D**

Limitations of current state

- Discretization of the model is not locally mass conservative
- Method of Lagrange multiplier

Open source software

- **Utopia** bitbucket.org/zulianp/utopia
- **ParMOONoLith** bitbucket.org/zulianp/par_moonolith

Institutions

Università della Svizzera italiana

Institute of Computational Science ICS

ETH zürich

GEG

CSCS
Centro Svizzero di Calcolo Scientifico
Swiss National Supercomputing Centre